ORNL/TM-6711

Electron-Beam Welding of Thorium-Doped Iridium Alloy Sheets

S. A. David
C. T. Liu
J. D. Hudson

OAK RIDGE NATIONAL LABORATORY
OPERATED BY UNION CARBIDE CORPORATION · FOR THE DEPARTMENT OF ENERGY

DISCLAIMER

Printed in the United States of America. Available from
National Technical Information Service
U.S. Department of Commerce
5285 Port Royal Road, Springfield, Virginia 22161
Price: Printed Copy $4.50; Microfiche $3.00

ORNL/TM-6711

Contract No. W-7405-eng-26

METALS AND CERAMICS DIVISION

ELECTRON-BEAM WELDING OF THORIUM-DOPED IRIDIUM ALLOY SHEETS

S. A. David, C. T. Liu, and J. D. Hudson

Date Published: April 1979

NOTICE This document contains information of a preliminary nature. It is subject to revision or correction and therefore does not represent a final report.

OAK RIDGE NATIONAL LABORATORY
Oak Ridge, Tennessee 37830
operated by
UNION CARBIDE CORPORATION
for the
DEPARTMENT OF ENERGY

THIS PAGE

WAS INTENTIONALLY

LEFT BLANK

CONTENTS

ELECTRON-BEAM WELDING OF THORIUM-DOPED IRIDIUM ALLOY SHEETS

S. A. David, C. T. Liu, and J. D. Hudson

ABSTRACT

Modified iridium alloys containing 100 ppm Th were found to be very susceptible to hot-cracking during gas tungsten-arc and electron-beam welding. However, the electron-beam welding process showed greater promise of success in welding these alloys, in particular Ir—0.3% W doped with 200 ppm Th and 50 ppm Al. The weldability of this particular alloy was extremely sensitive to the welding parameters, such as beam focus condition and welding speed, and the resulting fusion zone structure. At low speed successful electron-beam welds were made over a narrow range of beam focus conditions. However, at high speeds successful welds can be made over an extended range of focus conditions. The fusion zone grain structure is a strong function of welding speed and focus condition, as well.

In the welds that showed hot-cracking, a region of positive segregation of thorium was identified at the fusion boundary. This highly thorium-segregated region seems to act as a potential source for the nucleation of a liquation crack, which later grows as a centerline crack.

INTRODUCTION

Hot-cracking during welding has been a subject of a number of experimental studies.[1—4] A number of theories have been put forth to explain the mechanism of hot-cracking.[5—9] Hot-cracking often occurs during the later stages of solidification when the strains due to thermal and solidification contraction exceed the ductility of the partially solidified metal. Liquid pools trapped between the grains or interdendritic regions greatly influence the tensile properties of the partially solidified alloy. Also the mechanical behavior of the partially solidified alloy determines the hot-cracking sensitivity of the alloy.

Hot-cracking has been known to be favored by factors that decrease the solid-solid contact area during the last stages of solidification. Two of the most important factors are low-melting segregates and grain size. Low-melting segregates at the grain boundaries may exist as liquid film to temperatures well below the equilibrium solidus and reduce the grain boundary contact area to a minimum.[10] Also, the coarser the grain structure, the less the grain boundary contact area for a given amount of nonequilibrium liquid. Coarse-grained structures are generally more prone to hot-cracking than fine-grained structures.

A series of modified Ir—0.3% W alloys containing up to 500 ppm Th with substantially improved high-temperature impact properties over the Ir—0.3% W alloy have been developed at the Oak Ridge National Laboratory.[11] On evaluation of these modified alloys for fuel containers in radioisotope thermoelectric generators, alloys with at least 100 ppm Th have been found to be very sensitive to hot-cracking during gas tungsten-arc welding (GTAW) and electron-beam welding (EBW), Table 1. Of the two processes, EBW with its highly concentrated heat source and significantly lower heat input is more likely to produce a low-distortion weld. Further, the welding parameters during EBW can be controlled precisely. Preliminary weldability tests have shown that hot-cracking during EBW is extremely sensitive to the process variables, such as welding speed and beam focus conditions.

Table 1. Weldability Screening of Doped Iridium Alloys

Alloy	Dopants, ppm		Weld Process[a]	Results[b]
	Th	Al		
WTh-1	50		EB	no cracking
DOP-4-11D	30		EB	no cracking
DOP-23D		40	EB, GTA	no cracking
DOP-24D	30	100	EB, GTA	no cracking
DOP-25D	30	200	EB, GTA	no cracking
DOP-26C	60	60	EB, GTA	no cracking
DOP-22	100		EB, GTA	cracking
DOP-14	200		EB, GTA	cracking
DOP-27C	200	50	EB, GTA	cracking
DOP-28B	200		EB, GTA	cracking
DOP-21	500		EB, GTA	cracking

[a]Welds in 0.64-mm (0.025-in.) sheet; EB = electron beam, GTA = gas tungsten-arc welds in helium atmosphere chamber with lateral torch oscillation.

[b]All cracked specimens showed centerline cracking of the entire weld bead length.

EXPERIMENTAL PROCEDURE

Series of EB bead-on-plate welds were made on small 0.64-mm-thick coupons of DOP-27* with systematic variations in travel speed and beam focus condition. A Hamiltion Standard 6-kW electron-beam welder was used for the welding operations. The alloy sheet was fully recrystallized at 1500°C before welding. The operating conditions and results for autogenous bead-on-plate welds are summarized in Table 2. Series of welds with varying beam focus conditions at different speeds were made with constant beam voltage and slight variation in beam

*Ir—0.3% W doped with 200 ppm Th and 50 ppm Al. Aluminum is added to improve the high-temperature impact strength. It does not have any apparent effect on the weldability of the alloy.

Table 2. Electron-Beam Welding of Ir—0.3% W Alloy Doped with 200 ppm Th and 50 ppm Al

	Electron Beam		Travel Speed (mm/s)	Focusing numbers			Results		
	kv	MA		Sharp[a]	Used[b]	Defocusing[c]	Penetration	Appearance	Cracking Condition
1	116.0	5.0	2.5	727	734	7	full	overlapping spots	no
2	116.0	5.0	2.5	727	736	9	full	overlapping spots	no
3	116.0	5.0	2.5	727	737	10	full	smooth	no
4	116.0	5.0	2.5	727	739	12	full	smooth	no
5	116.0	5.0	2.5	727	741	14	full	smooth	no
6	116.0	5.0	2.5	727	743	16	partial	smooth	no
7	116.4	4.8	4.1	720	730	10	full	overlapping spots	no
8	116.4	4.8	4.1	720	731	11	full	overlapping spots	no
9	116.4	4.8	4.1	721	734	13	full	overlapping spots	no
10	116.4	4.8	4.1	721	735	14	full	smooth	no
11	116.4	4.8	4.1	717	732	15	full	smooth	no
12	116.4	4.8	4.1	718	734	16	full	smooth	no
13	116.4	4.7	4.1	721	738	17	full	smooth	cracked
14	116.4	4.0	4.1	718	736	18	full	smooth	cracked
15	116.0	6.0	6.4	717	728	11	full	overlapping spots	no
16	115.9	6.0	6.4	720	735	15	full	overlapping spots	no
17	115.9	6.0	6.4	721	737	16	full	smooth	no
18	115.9	6.0	6.4	720	737	17	full	smooth	no
19	115.9	6.0	6.4	717	735	18	full	smooth	no
20	115.9	6.0	6.4	720	739	19	full	smooth	no
21	115.9	6.0	6.4	720	741	21	partial	smooth	no
22	115.9	6.0	6.4	720	743	23	partial	smooth	no
23	116.5	7.1	8.5	721	735	14	full	overlapping spots	no
24	116.5	7.1	8.5	721	736	15	full	smooth	no
25	116.5	7.1	8.5	720	740	20	full	smooth	no
26	116.5	7.1	8.5	721	743	22	full	smooth	no
27	116.5	7.1	8.5	721	745	24	full	smooth	cracked
28	116.0	8.0	12.7	716	720	4	full	overlapping spots	no
29	116.0	8.0	12.7	716	723	7	full	overlapping spots	no
30	116.0	8.0	12.7	716	726	10	full	smooth	no
31	116.0	8.0	12.7	716	731	15	full	smooth	no
32	116.0	8.0	12.7	716	736	20	full	smooth	no
33	116.0	8.0	12.7	716	741	25	full	smooth	no
34	116.0	8.0	12.7	716	746	30	full	smooth	no

[a] Sharp focusing current.
[b] Focusing current used for welding.
[c] (Focusing current used for welding) − (sharp focusing current).

current. The welding speed varied from 2.5 to 12.7 mm/s. The spot size of the beam was controlled by varying the focus number, an arbitrary digital reading that is related is the focus coil current. The focus control number was varied 20 digits above sharp focus on the sheet surface (approximately 50 mm above the sheet) and 30 digits below sharp focus on the sheet surface (approximately 75 mm below the sheet). The beam focus condition used for each weld may be estimated from the difference between the sharp focus control number and the focus control number used for welding. The work distance was maintained constant at 0.22 m. Various sections of the welds were prepared for metallographic observations by standard techniques. The samples were etched electrolytically in a solution of 400 ml H_2O, 100 ml HCl, and 50 g NaCl with a stainless steel cathode.

RESULTS AND DISCUSSION

Beam Focusing

Weldability of DOP-27 was found to be extremely sensitive to the welding speed and focus conditions. These factors influence the macroscopic appearance of the weld bead. Figure 1 shows the results of

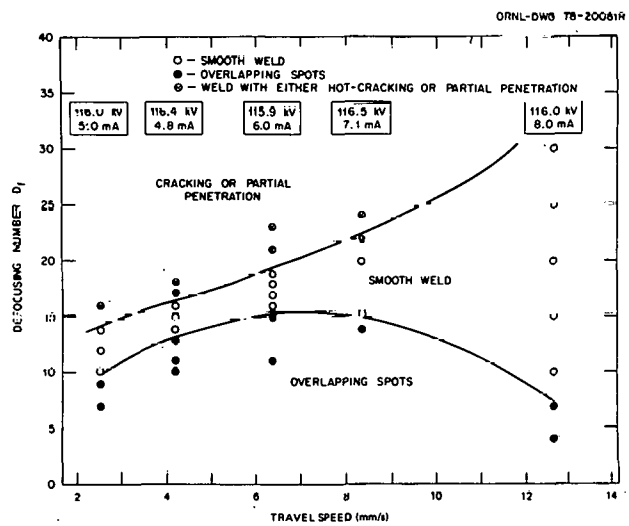

Fig. 1. Weldability of Doped Iridium Alloy DOP-27 as a Function of Defocusing Number and Travel Speed.

a number of welds made at various welding speeds and focus conditions. For a given beam voltage, current, and welding speed, the bead appearance varied with the extent of defocusing D_f (difference between sharp focusing number and focusing number used for welding). For focusing conditions at or near sharp focus the weld bead length contained a series of holes punched in the sheet [Fig. 2(a)]. A possible reason for this is that close to the sharp focus the electron beam could produce such intense local heating that it almost instantly vaporizes the metal locally, producing a hole. On defocusing the beam, the weld bead length appeared to contain a series of overlapping spot welds (designated as rough weld for discussion purposes), Fig. 2(b). However, a careful metallographic examination of the sample revealed continuous melting all along the bead length. Further defocusing produced a smooth weld with full penetration [Fig. 2(c)]. Such successful welds were made over a narrow range of focus conditions. Focus conditions above this range, resulted in either hot-cracking or lack of full penetration. However, increasing the welding speed further extended the range of focus conditions over which successful welds were made. This trend is clearly shown in Fig. 1. Since the beam current varied slightly for the series of welds made at different welding speeds, it is likely that this could have some influence on the range of focus conditions over which successful welds can be made. However, a series of welds made at constant beam voltage and current showed that the major influence on the critical range of focus conditions was due to the increase in welding speed. Also, the results obtained were identical for sharp focus below or above the sheet surface. Perhaps this probably is due to the very small thickness of the sample involved. During EBW of heavy sections, conditions of overfocusing or underfocusing do influence penetration.

Y-157542

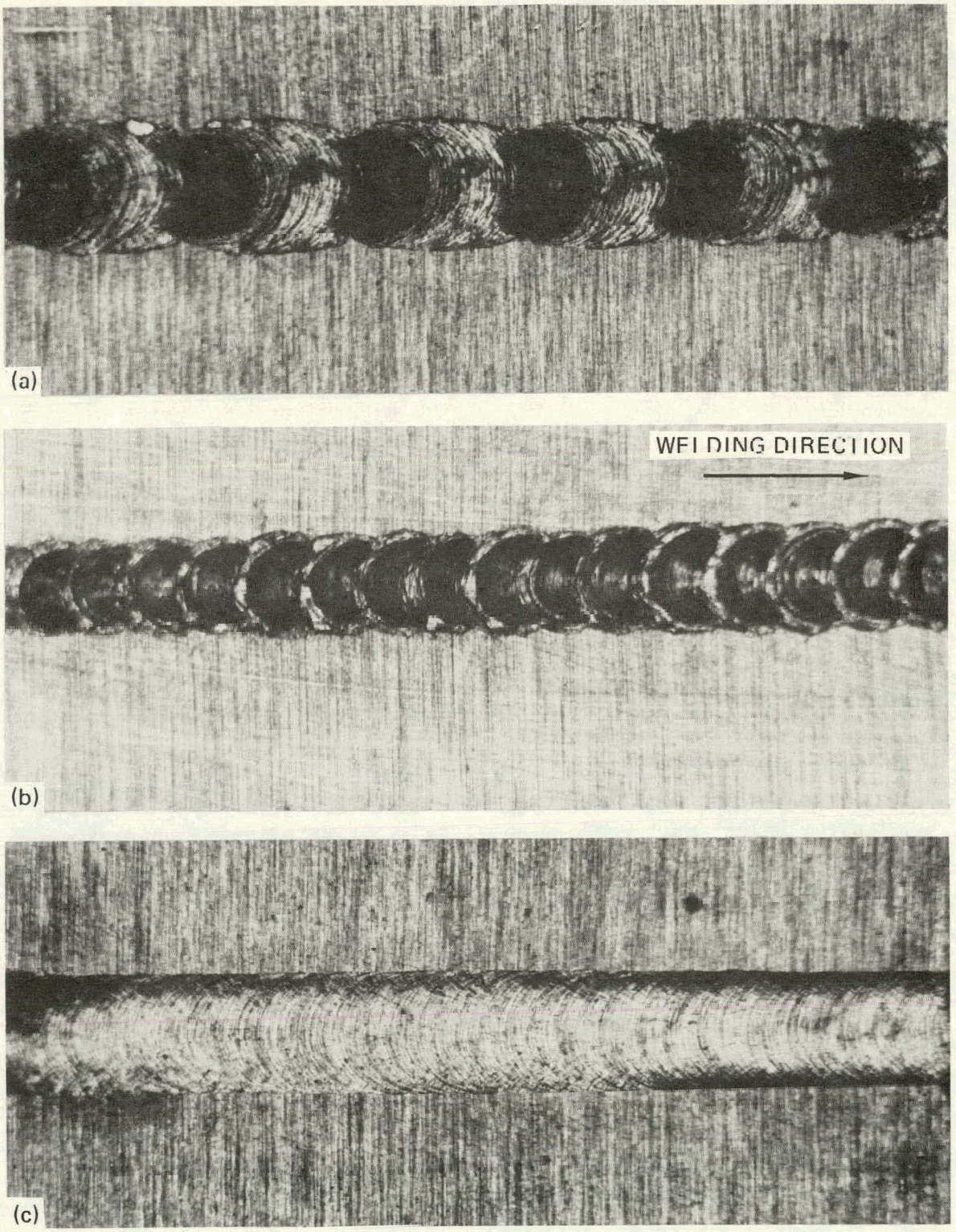

Fig. 2. As-Welded DOP-27 Specimens with a Travel Speed of 2.5 mm/s and Various Focus Conditions. 12×. (a) Defocusing number D_f = 7. (b) D_f = 9. (c) D_f = 12.

Microstructure

Figure 3 shows typical microstructures of a successful smooth weld obtained at a low welding speed (1.7 mm/s). The puddle shape at this welding speed has been observed to be nearly circular (ratio of the major to minor axes of the ellipse is close to 1). The fusion zone revealed a fine grain structure. However, the substructure within the grains is not clearly visible because of etching difficulties, and when visible it has been observed to be cellular or dendritric. Further, the fusion zone structure revealed epitaxial growth of partially melted grains in the base metal sheet, Fig. 3(a). In general, during welding the initial growth of partially melted grains in the base metal is followed by a competitive growth process resulting from the tendency for growth to proceed most readily in grains oriented along that easy growth direction having the largest component of the temperature gradient.[12–14] For both fcc and bcc materials (iridium is fcc) ⟨ 100 ⟩ directions are the easy growth directions.[15] However, since the maximum temperature gradient is normal to the pool boundary and in our work the puddle is nearly circular, the direction of the temperature gradient changes continuously from the fusion boundary to the weld centerline. Hence, no single grain experiences favored growth for any extended period. Since the grain structure of the base metal is very fine, many of these grains starting from the fusion boundary survive to reach the center of the weld, as shown in Fig. 3(a), hence, the observed fine grain structure in the fusion zone at low welding speeds. The grains surviving over an extended distance also show considerable curvature due to the progressive change in the preferred growth direction [Fig. 3(a)]. Similar fusion zone grain structure development was also observed in the welds [Fig. 2(b)] produced at focus conditions close to sharp focus and low welding speed.

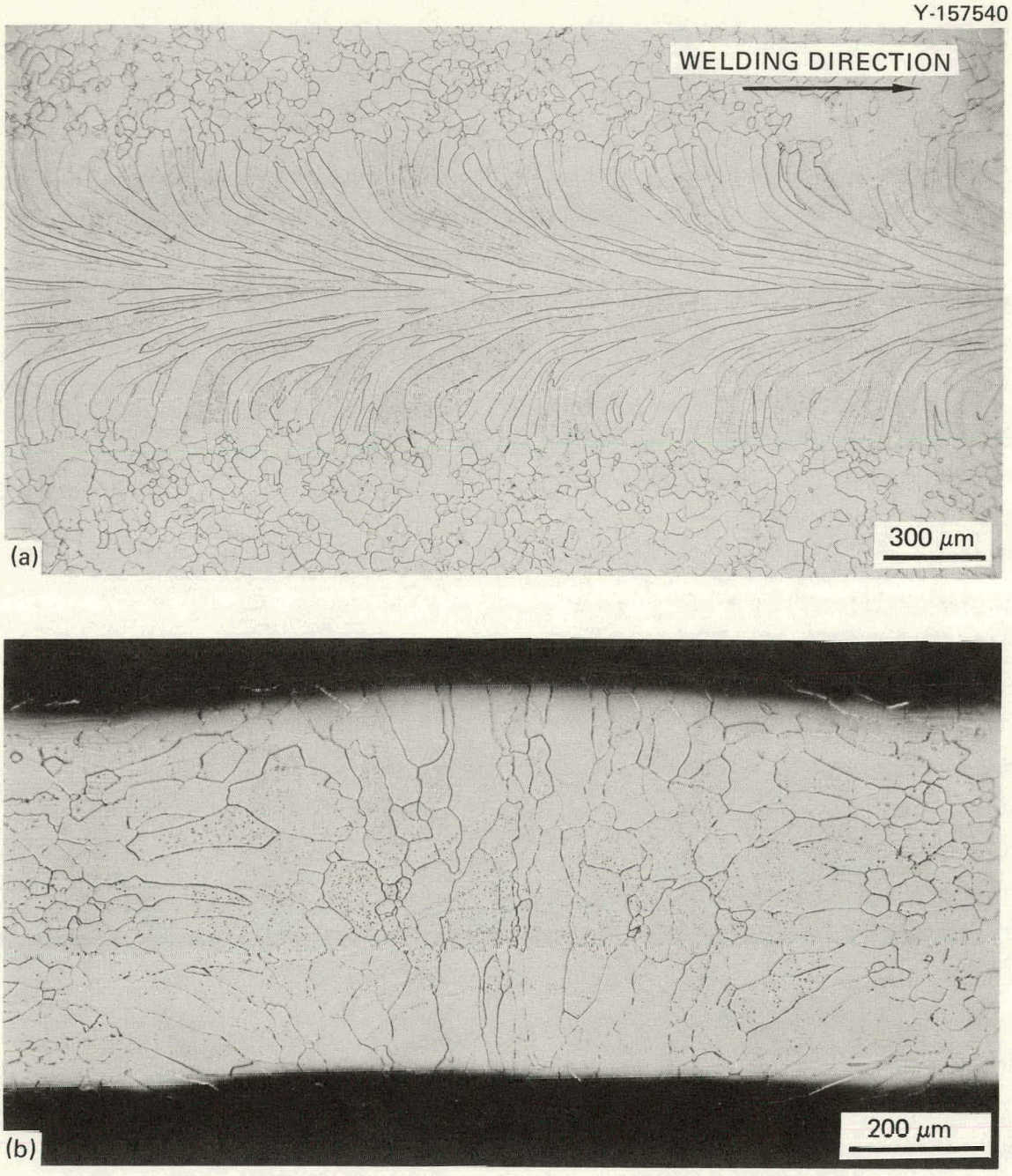

Fig. 3. Fusion Zone Microstructures of an Electron-Beam Weld Showing a Fine Grain Structure. Travel speed 2.5 mm/s and defocusing number D_f = 12. (a) Top surface. (b) Transverse section.

Figure 4 shows typical microstructures of a smooth weld obtained at moderate traveling speed (6.4 mm/s). The puddle shape at this speed appears to be elliptical. Unlike the structure of the welds obtained at low speed, the fusion zone revealed a rather coarse grain structure. Many of the partially melted grains starting from the fusion boundary did not survive to reach the center of the fusion zone [Fig. 4(a)]. Of the many grains growing along the welding direction, a few that are oriented favorably appear to outgrow the unfavorably oriented grains, so the fusion zone structure is coarse. Often one or two grains spanned the thickness of the weld at its center. A structure such as this is very much prone to cracking. However, the fusion zone structure of a rough weld produced with focusing conditions close to sharp focus and at moderate speeds contained a fine grain structure. This may be due to the violent stirring action of the puddle during welding close to the sharp focusing conditions and subsequent grain refinement.

Typical microstructures of a smooth weld obtained at high speed (12.7 mm/s) are shown in Fig. 5. The fusion zone contained a fine grain structure. Also, the puddle shape at this speed continues to be elliptical. As at moderate speeds, many of the partially melted grains starting from the fusion boundary did not survive to reach the center of the fusion zone [Fig. 5(a)]. However, the grains growing along the welding direction were fine because of the high solidification rate. Also conformance to easy growth direction decreases as freezing rate increases.

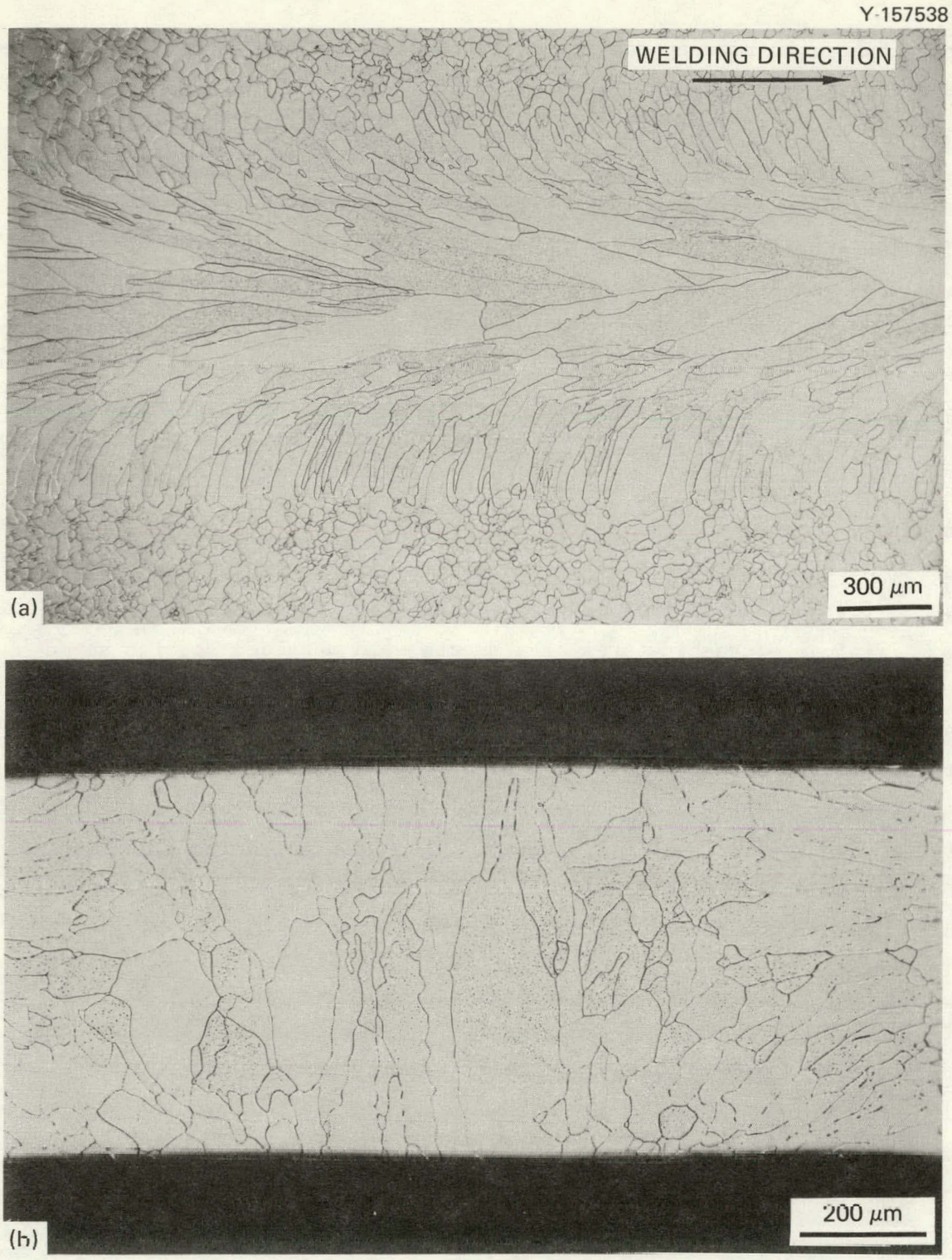

Fig. 4. Fusion Zone Microstructures of Electron-Beam Weld Showing a Coarse Grain Sructure. Travel speed 6.4 mm/s and defocusing number D_f = 18. (a) Top surface. (b) Transverse section.

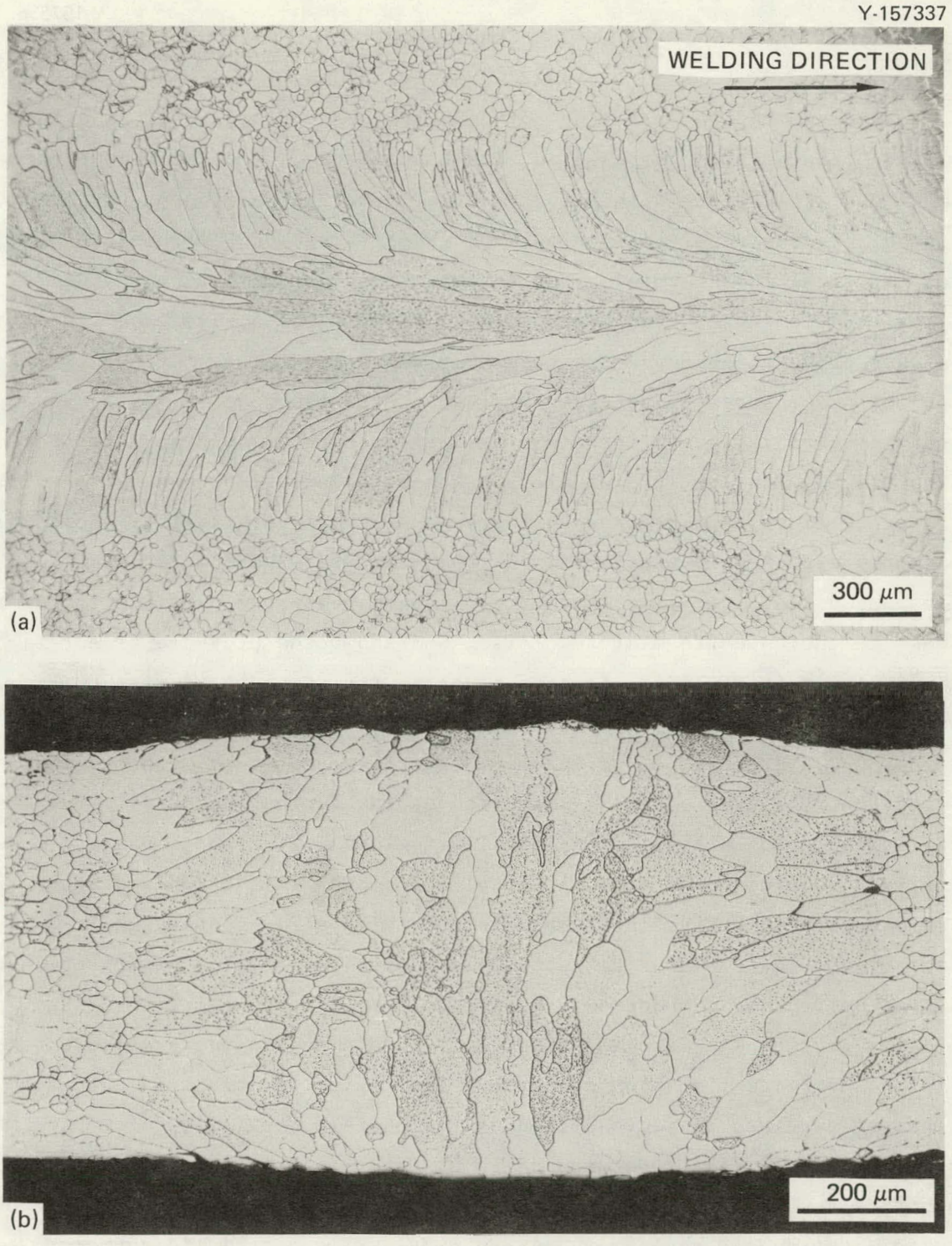

Fig. 5. Fusion Zone Microstructures of an Electron-Beam Weld Showing a Fine Brain Structure. Travel speed 12.7 mm/s and defocusing number D_f = 20. (a) Top surface. (b) Transverse section.

Hot-Cracking

As discussed earlier, the hot-cracking susceptibility of an alloy depends on elemental composition, its distribution, and the microstructural characteristics within the material. During welding of the iridium alloy, the resulting fusion zone grain structure was found to be very critical in determining the hot-cracking susceptibility of the alloy. Fusion zone structures shown in Figs. 3 and 5 have been found to be less prone to hot-cracking than that shown in Fig. 4. With thermal and shrinkage stresses acting normal to the fusion zone, a fusion zone containing coarse grain structure is very much prone to cracking. During EBW, cracking in the iridium alloy has been found predominantly to follow the centerline. The crack path has been mostly intergranular. Scanning electron microscopic examination of the fractured surface revealed the presence of eutectic-like structure,[16] Ir_5Th being the possible second phase in the eutectic mixture. Also, SEM shows the presence of a relatively low-melting liquid (eutectic) along the grain boundaries during later stages of solidification, due to solute segregation.

A close observation of the microstructure and crack path has indicated that the crack, having initiated at the fusion boundary, works its way to the weld centerline and finally follows it. Figures 6 and 7 show the macroscopic and microscopic details of crack initiation and subsequent growth pattern in an EB welded iridium alloy containing Ir—0.3% W and 500 ppm Th. On analyzing the weld sample for thorium distribution by a spark-source mass spectrometric method a region of positive segregation of thorium was detected (Fig. 8). Such a region has a great potential to nucleate liquation cracking. The region of positive segregation observed here may be rationalized on the basis of bulk flow of solute-enriched liquid between cells or dendrite arms in a direction opposite to that of the solidification front to feed volume shrinkage on solidification and cooling.[17] A phenomenon such as this is commonly observed during ingot solidification. Also, thorium migration to the fusion boundary under the influence of a steep thermal gradient could enhance the thorium level at the fusion boundary. Welding speed may

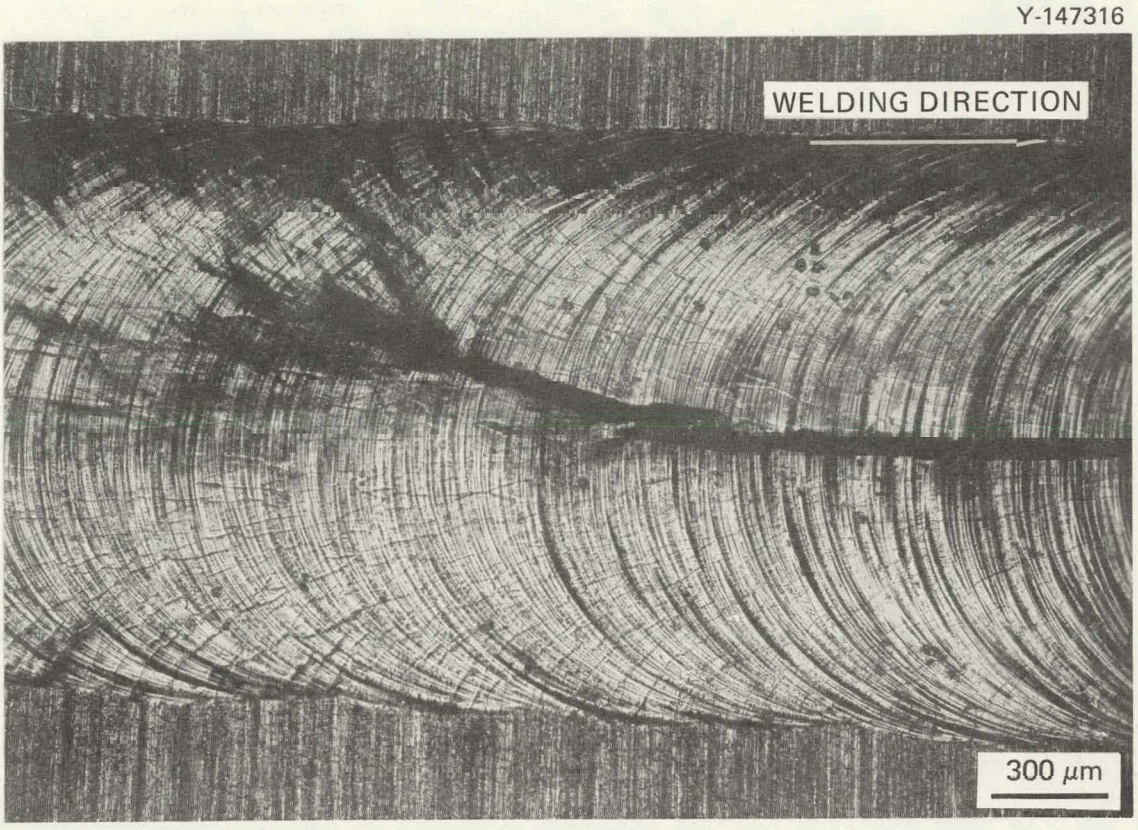

Fig. 6. Details of Crack Path in an Electron-Beam Weld.

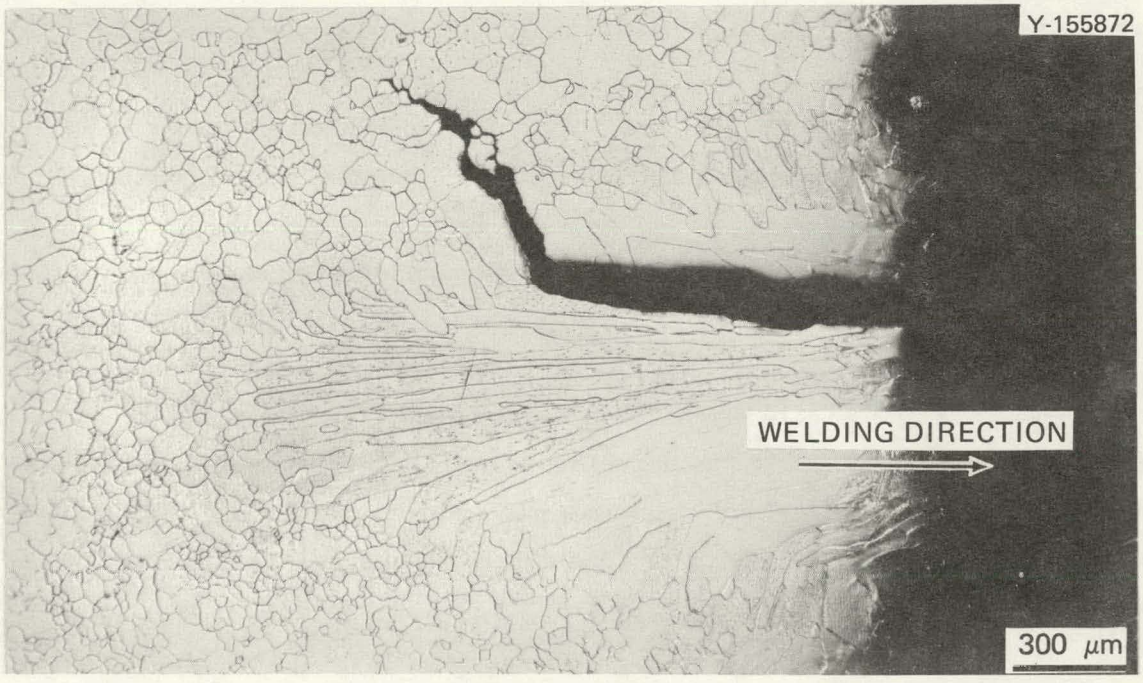

Fig. 7. Crack Nucleation at the Fusion Boundary and Further Propagation as a Centerline Crack.

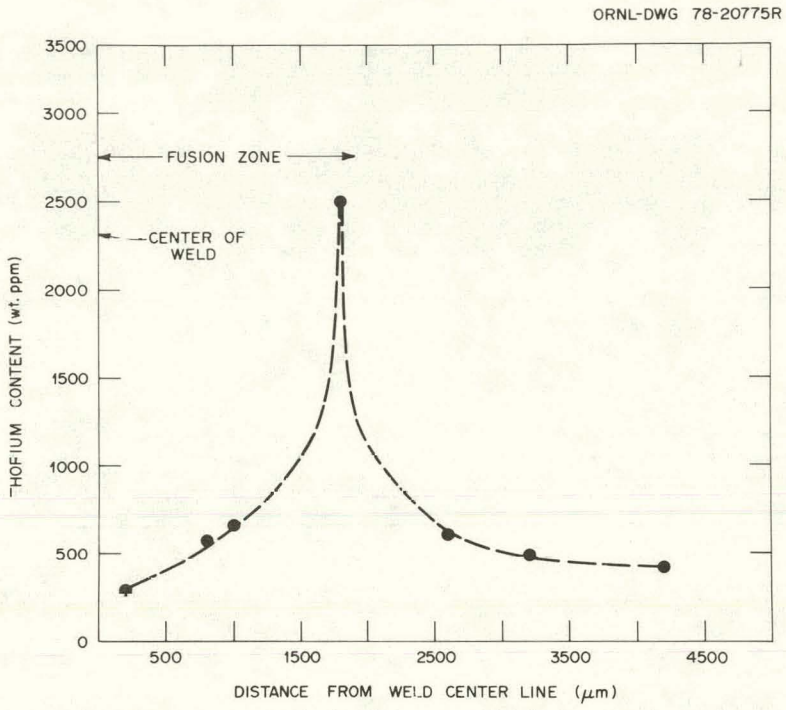

Fig. 8. Concentration of Thorium as a Function of a Distance From the Weld Centerline in Electron-Beam-Welded DOP-21 Alloy.

have a great influence on these factors in that the segregation of thorium may be less severe at high welding speeds than at low welding speeds. Hence, the combination of least segregation and fine fusion zone grain structure at high welding speeds seems to improve the weldability, as shown in Fig. 1.

CONCLUSIONS

Electron-beam welding shows great promise of success in welding the modified iridium alloys, in particular Ir—0.3% W doped with 200 ppm Th and 50 ppm Al. Electron-beam welding parameters to successfully weld thin sheets of this alloy have been established. Weldability of this particular alloy is a strong function of welding parameters, such as welding speed and beam focus conditions. The alloy can be welded successfully over a range of focus conditions, the range being narrow at low welding speeds and extended at high welding speeds.

The fusion zone grain structure has been found to be a strong function of welding speed and focus conditions as well. Fusion zone grain structure was fine at low and high speeds and coarse at moderate speeds. Also the fusion zone grain structure is closely related to the hot-cracking susceptibility of the alloy.

A region of positive segregation in thorium was identified at the fusion boundary in the welds that exhibited hot-cracking. This region acts as the potential source for the nucleation of a liquidation crack that reaches the centerline and further grows as a centerline crack.

ACKNOWLEDGMENTS

The authors gratefully acknowledge the encouragement of A. C. Schaffhauser as program manager. Also the authors wish to acknowledge G. M. Goodwin for his guidance and suggestions during the initial course of this investigation and J. F. King and C. J. Long for technical review and C. P. Haltom for metallography. Thanks are also extended to S. Peterson for editing and K. A. Witherspoon for typing the manuscript.

REFERENCES

1. P. P. Puzak, W. R. Apblett and W. S. Pellini, "Hot Cracking of Stainless Steel Weldments," *Weld J. (New York)* 35(1): 96-s–175-s (1956).
2. W. R. Apblett and W. S. Pellini, "Factors Which Influence Weld Hot Cracking," *Weld. J. (New York)* 33(2): 83-s–90-s (1954).
3. J. C. Borland, "Hot Cracking in Welds," *Br. Weld. J.* 7: 558–59 (1960).
4. F. C. Hull, "Effect of Delta Ferrite on the Hot Cracking of Stainless Steel," *Weld J. (New York)* 399-s–409-s (1967).
5. J. Vero, *Met. Ind. (London)* 48: 431–37 (1936).
6. A.R.E. Singer and P. H. Jennings, "Properties of the Al-Si 1035 Alloys at Temperatures in the Region of the Solidus," *J. Inst. Met.* 73: 33–54 (1946).

7. A.R.E. Singer and P. H. Jennings, "Hot-Shortness of Some High Purity Alloys," *J. Inst. Met.* 74: 227–40 (1947).
8. W. S. Pellini, *Foundry* 80: 124–33 (1952).
9. J. C. Borland, "Generalized Theory of Super Solidus Cracking in Welds and Castings," *Br. Weld. J.* 7: 508–12 (1960).
10. C. S. Smith, "Grains, Phases and Interfaces," *Trans. AIME* 175: 15–51 (1948).
11. C. T. Liu and H. Inouye, *Development and Characterization of an Improved Ir–0.3% W Alloy for Space Radioisotopic Heat Source,* ORNL-5290 (October 1977).
12. W. F. Savage and A. H. Aronson, "Preferred Orientation in the Fusion Zone," *Weld. J. (New York)* 45(2): 855-s–895-s (1966).
13. W. F. Savage, C. D. Lundin, and R. J. Hrubec, "Segregation and Hot-Cracking in Low-Alloy Quench and Tempered Steels," *Weld. J. (New York)* 47(9): 420-s–425-s (1968).
14. G. J. Davies and J. G. Garland, "Solidification Structure and Properties of Fusion Welds," *Int. Metall. Rev.* 20: 83–105 (1975).
15. A. Hellawall and P. M. Herbert, *Proc. R. Soc. London, Ser. A* 269: 560 (1962).
16. C. L. White, Oak Ridge National Laboratory, private communication.
17. J. S. Kirkaldy and W. V. Youdelis, "Contribution to the Theory of Inverse Segregation," *Trans. Metall. Soc. AIME,* 212: 833 (1958).

INTERNAL DISTRIBUTION

1–2.	Central Research Library	24–26.	M. R. Hill
3.	Document Reference Section	27.	H. Inouye
4–5.	Laboratory Records Department	28.	J. R. Keiser
6.	Laboratory Records Department, RC	29.	J. F. King
7.	ORNL Patent Section	30.	C. T. Liu
8.	P. Angelini	31.	J. W. McEnerney
9–18.	S. A. David	32.	H. E. Reesor
19.	D. P. Edmonds	33–37.	A. C. Schaffhauser
20.	G. M. Goodwin	38.	J. E. Selle
21.	R. J. Grey	39.	R. L. Shoup
22.	D. E. Harasyn	40.	G. M. Slaughter
23.	R. Heestand	41.	C. F. Yen

EXTERNAL DISTRIBUTION

42–53. DOE Division of Advanced Systems and Materials Production, Washington, DC 20545

R. C. Brouns	R. B. Morrow
T. J. Dobry	P. A. O'Riordan
N. Goldenberg	W. C. Remini
J. S. Griffo	B. J. Rock
W. D. Kenney	C. O. Tarr
J. J. Lombardo	N. R. Thielke

54–55. DOE Albuquerque Operations Office, P.O. Box 5400, Albuquerque, NM 87115

D. K. Nowlin
D. Plymale

56. DOE Oak Ridge Operations Office, P.O. Box E, Oak Ridge, TN 37830

Assistant Manager, Energy Research and Development

57–83. DOE Technical Information Center, P.O. Box 62, Oak Ridge, TN 37830

84–85. DOE San Francisco Operations Office, 1333 Broadway, Wells Fargo Building, Oakland, CA 94612

L. Lanni
W. L. Von Flue

86–87. DOE Savannah River Operations Office, P.O. Box A, Aiken, SC 29801

W. T. Goldston
W. D. Sandberg

88. DOE Dayton Area Office, P.O. Box 66, Miamisburg, OH 45342

H. N. Hill

89. E. I. du Pont de Nemours, Savannah River Plant, Aiken, SC 29801

R. A. Brownback

90. E. I. du Pont de Nemours, Savannah River Laboratory, Aiken, SC 29801

R. T. Huntoon

91–92. Fairchild Industries, 20301 Century Blvd., Germantown, MD 20767

M. Eck
A. Schock

93–94. General Electric Co., Valley Forge Space Center, P.O. Box 8048, Philadelphia, PA 19101

E. H. Sayell
E. W. Williams

95–96. Jet Propulsion Laboratory, California Institute of Technology, 4800 Oak Grove Drive, Pasadena, CA 91103

J. E. Mondt
A. E. Wolfe

97–99. Los Alamos Scientific Laboratory, P.O. Box 1663, Los Alamos, NM 87545

R. D. Baker
S. E. Bronisz
S. S. Hecker

100–103. Minnesota Mining and Manufacturing Co., St. Paul, MN 55101

R. B. Ericson
E. F. Hampl
W. C. Mitchell
R. S. Reylek

104. Monsanto Research Corp., P.O. Box 32, Miamisburg, OH 45342

E. W. Johnson

105. Sundstrand Energy Systems, 4747 Harrison Ave., Rockford, IL 61101

E. Krueger

106–110. Teledyne Energy Systems, 110 W. Timonium Rd., Timonium, MD 21093

W. J. Barnett
M. I. Haar
A. R. Lieberman
W. E. Osmeyer
F. A. Schumann

☆U.S. GOVERNMENT PRINTING OFFICE: 1979-640-079/16